INSTITUTE OF PHYSICS PUBLISHING JOURNAL OF PHYSICS: CONDENSED MATTER

J. Phys.: Condens. Matter **17** (2005) 619–634 doi:10.1088/0953-8984/17/4/005

Nanoscale defect structures at crystal–glass interfaces

S V Bobylev[1], I A Ovid'ko[1], A E Romanov[2] and A G Sheinerman[1]

[1] Institute for Problems of Mechanical Engineering, Russian Academy of Sciences, Bolshoj 61, Vasilyevsky Ostrov, St Petersburg 199178, Russia
[2] Ioffe Physico-Technical Institute, Russian Academy of Sciences, Polytechnicheskaya 26, St Petersburg 194021, Russia

E-mail: ovidko@def.ipme.ru

Received 19 August 2004, in final form 17 December 2004
Published 14 January 2005
Online at stacks.iop.org/JPhysCM/17/619

Abstract

A theoretical model of two-phase crystal–glass composite materials is suggested which is based on the disclination description of glassy structures. In the framework of the model, the crystal–glass composite is described as a solid that contains nanoscale configurations of disclination–dislocation loops in the glassy phase. Specific defects at the crystal–glass interface are defined and theoretically described which are misfit disclinations generated as extensions of parent wedge disclinations present in the glassy phase. In doing so, the defect ensemble in the crystal–glass composite is characterized by nanoscale inhomogeneities in both the defect density and stress in the vicinity of the crystal–glass interface. The formulae for the stress fields created by ensembles of the disclination–dislocation loops in crystal–glass composites are derived. With these formulae, the energy of the crystal–glass interface is estimated.

1. Introduction

Crystal–glass composite materials (bulk composites consisting of crystallites embedded in an amorphous matrix, bulk composites consisting of amorphous particles embedded in a crystalline matrix, multilayer coatings, nanocomposite coatings consisting of nanocrystallites divided by amorphous intergranular layers, amorphous thin films on crystalline substrates, crystalline thin films on amorphous substrates, etc) represent the subject of intense experimental and theoretical research efforts motivated by a wide range of their applications in high technologies; see, e.g., [1–19]. Physical and mechanical properties of these composite materials essentially depend on both the structure and behavior of crystal–glass interfaces. In particular, the role of crystal–glass interfaces is crucial in physical processes occurring in nanocrystal–glass composite materials [15, 16] where the volume fraction of the interfacial phase is very large. The aforesaid causes a high interest in understanding and a theoretical description of the specific structural and behavioral peculiarities of crystal–glass interfaces.

 © 2005 IOP Publishing Ltd Printed in the UK

One of the most important characteristics of a crystal–glass interface is its energy. For instance, the interface energy serves as a key parameter regulating both crystal-to-glass and glass-to-crystal transformations [1–3, 17–19]. Benedictus *et al* [20] have estimated the energy of crystal–glass interfaces in the framework of the thermodynamic approach, which, however, does not take into account the misfit (geometric mismatch inducing distortions) between the amorphous and crystalline phases. At the same time, the misfit accumulated at interphase boundaries is known to definitely influence their properties, even if both the phases adjacent to the interphase boundary are crystalline ones with similar structures; see, e.g., [21–26]. Since the very different crystalline and amorphous phases are matched at crystal–glass interfaces, it is natural to expect that their specific features are a high misfit between the shared phases and, as a corollary, the existence of high-density ensembles of misfit defects (defects associated with misfit) at such interfaces. In the letter [27] the representations on misfit disclinations as defects associated with orientational misfit between the adjacent amorphous and crystalline phases have been introduced and briefly discussed. The main aim of this paper is to elaborate a detailed theoretical description of misfit defect structures in crystal–glass composites and estimate the specific energy of the interfaces between the crystalline and amorphous phases with the same chemical composition. In doing so, the focuses are placed on the misfit disclinations briefly discussed earlier [27] and nanoscale configurations of disclination–dislocation loops at crystal–glass interfaces.

2. Structural geometry of crystal–glass interfaces. Misfit disclinations

Let us consider crystal–glass interfaces between the amorphous and crystalline phases. For definiteness, in our analysis of crystal–glass interfaces, hereinafter we restrict our consideration to the situation with both the crystal and the glass having the same topology of facets as most of their elementary units (atomic clusters). This allows adjacent crystalline and glassy surfaces to be partly matched in a coherent way at a crystal–glass interface. Such interfaces, at the same time, contain topological misfit defects that locally (at defect cores) violate the coherent matching. The interfaces between metallic glasses and crystals with bcc and fcc lattices serve as a characteristic example, because the facets of elementary units—tetrahedral and octahedral pyramids—of both metallic glasses and bcc (fcc) crystals have the topology of triangles and rectangles that are facets of these pyramids (figure 1); see, e.g. [28]. In the following, for definiteness, we will focus our consideration on metallic glass–crystal interfaces and just briefly discuss the case of covalent glass–crystal interfaces.

In general, the common features of covalent and metallic glasses are the absence of a long-range translational order, and the existence of a short-range orientational order, intermediate-range homogeneity and frozen-in local distortions in the glassy structure. These features and the properties exhibited by glasses are effectively described within the framework of the disclination models (e.g., [29–32]), that treat glasses as solids with disorderedly distributed disclination defects destroying the long-range orientational order and being responsible for the local distortions in glasses. Such disclinations commonly form low-energy configurations with screened stress fields [29–32]; this reflects the intermediate-range homogeneity inherent to a (disclinated) glass. In the case of metallic glasses described as disclinated solids [30], there are two types of disclination: continuously distributed disclinations characterized by small negative values of disclination strength and isolated disclinations characterized by large positive values of disclination strength. The continuously distributed disclinations of small negative strength are associated with the spontaneous continuous curvature of the glassy structures, which is due to short range interactions [30]. The isolated disclinations of large positive strength play the role of defects that compensate for the spontaneous continuous curvature associated

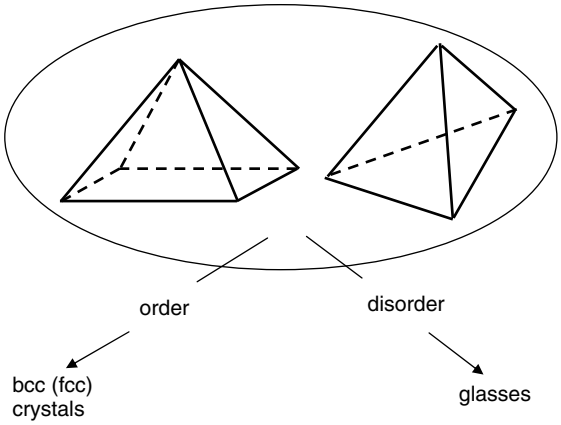

Figure 1. Tetrahedral and octahedral pyramids, which serve as structural units of both metallic bcc (fcc) crystals and glasses characterized by long- and short-range order in their arrangement, respectively. Facets of tetrahedra and octahedral pyramids are triangles and rectangles. These facets are matched at crystal–glass interfaces.

with small-strength disclinations. In terms of curvature, large-strength disclinations provide the flattening of the disclinated glassy structures to be embedded in the real three-dimensional space [30]. The disclination approach is also effective in a description of covalent glasses as solids with disclinations of both positive and negative strength. For instance, disclinations are defined as the line defects threading the internal regions of the five- and seven-sided rings of atoms in the glassy phase of covalent structures whose crystal phase contains the six-sided rings of atoms [30]. In doing so, disclinations serve as carriers of internal curvature in covalent glasses, as with metallic glasses [30, 31].

Also, the disclination models of the glassy (amorphous) structures are effective in a theoretical description of stress fields and plastic deformation processes in such structures [30–32]. With this taken into account, we will use the disclination approach in our further analysis of misfit defects and stresses generated at crystal–glass interfaces.

Let us consider a crystal–glass interface resulting from the matching of a crystal and a glass, being a solid with disclinations threading its bulk and entering its surface (figure 2(a)). According to the disclination charge (Frank pseudo-vector) conservation law [30, 31], no disclination can terminate in the bulk of a solid; disclinations either terminate at a free surface or form loop configurations in the bulk of a solid. As a corollary, after the crystalline and glassy surfaces have been matched, the disclinations previously (before matching) terminated at the pre-existent free surface of the glass have to be transformed and extended in the new crystal–glass composite. More precisely, in order to satisfy the disclination charge conservation law in the new crystal–glass composite, the disclinations have to be extended to the crystal–glass interface [27] (figure 2(b)).

Notice that misfit disclinations at crystal–glass interfaces (figure 2(b)) are associated with orientational mismatch between the glassy phase specified by a short-range orientational order and the adjacent crystalline phase characterized by a long-range orientational order. More precisely, elementary atomic clusters at the contact surfaces of the adjacent glassy and crystalline phases are misoriented relative to each other, when they match and form a crystal–glass interface. In doing so, the local misorientation between the matching atomic clusters is spatially inhomogeneous, because the clusters at the contact surface of the crystalline phase (having a long-range orientational order) are oriented identically, while orientation of

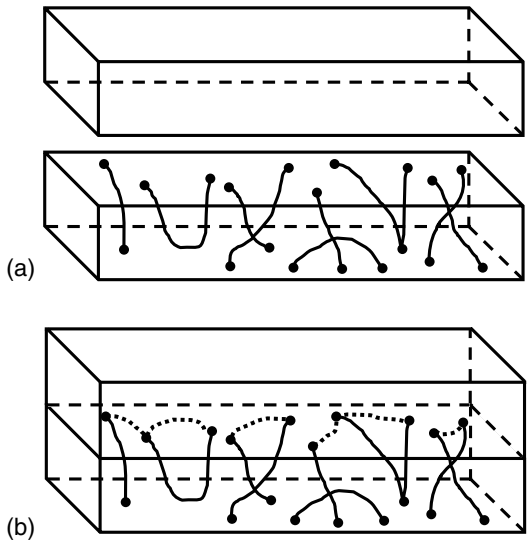

Figure 2. Formation of a crystal–glass composite. (a) A crystal (top layer) and a glass (bottom layer) with parent wedge disclinations (solid lines terminated by full circles on surfaces of the bottom layer) before their matching. (b) After the crystal and the glass have been matched, parent disclinations extend from the glass to the crystal–glass interface at which misfit twist disclinations (dotted lines) are formed.

the clusters at the contact surface of the amorphous phase (characterized by a short-range orientational order) is spatially inhomogeneous. In the framework of our approach, misfit disclinations as rotational defects inducing spatially inhomogeneous stress fields play the role of carriers of the spatially inhomogeneous orientational mismatch at crystal–glass interfaces. In general, similar misfit defect structures—misfit disclinations at low- and high-angle grain boundaries—are formed also in polycrystalline and nanocrystalline films deposited onto single-crystalline substrates; see experimental data [33, 34] and theoretical models [24, 35]. In this situation, misfit disclinations are associated with orientational mismatch between misoriented grains of a film and a single-crystalline substrate. In addition to these disclinations located at interphase boundaries, there are disclinations located at grain boundaries in single-phase polycrystalline and nanocrystalline materials. Such grain boundary disclinations are treated as defects providing misorientation (in other terms, orientational misfit) between adjacent grains of the same crystal phase [31, 36–38].

In parallel with the orientational misfit between the adjacent glassy and crystalline phases, there exists a dilatation misfit related to the difference between the characteristic interatomic distances in the adjacent glassy and crystalline phases. The dilatation misfit at crystal–glass interfaces is similar to that at conventional crystal–crystal interfaces. Therefore, it is effectively described in terms of the dilatation misfit parameter and associated dilatation misfit stresses and misfit dislocations; see, e.g., reviews [21–23]. Since a description of the dilatation misfit is a standard procedure, here and in the following we will focus our consideration on a description of only the orientational misfit and associated misfit disclinations at crystal–glass interfaces.

Thus, the matching of the glassy and crystalline phases results in the formation of the special misfit defects at the crystal–glass interface. By definition, such defects are located in the interface plane and originate at the end points of the wedge disclinations entering the interface (figure 2(b)). As extensions of parent disclinations, the special misfit defects are misfit

disclinations characterized by the same Frank pseudo-vectors $\boldsymbol{\omega}$ as their parent disclinations. However, the lines of the special misfit defects lying in the interface plane are bent relative to the lines of their parent disclinations and, as a corollary, their characteristic vectors $\boldsymbol{\omega}$. This causes the types of misfit disclinations to be different from the types of parent disclinations. In particular, wedge disclinations in the glassy phase are extended to form misfit disclinations of the twist type at the crystal–glass interface.

In the framework of the suggested approach, the crystal–glass interfaces are effectively represented as semi-coherent interfaces with coherent fragments and high-density ensembles of misfit disclinations. This representation will allow us to describe theoretically the characteristics—in particular, elastic energy density—of crystal–glass interfaces as those of ensembles of misfit defects (see the next sections). On the other hand, the crystal–glass interfaces represented as semi-coherent interfaces contain coherent fragments with one-to-one atomic matching. In the case discussed, such interfaces have to be sensitive to crystallographic peculiarities of the adjacent crystalline phase. In this context, the experimental observations of facetted crystal–glass interfaces [10, 11] and pronounced textures in polycrystalline films on glassy substrates [12] support the theoretical representations elaborated here.

3. Disclination–dislocation ensemble in crystal–glass composite. Model

In order to quantitatively estimate the specific elastic energy of a crystal–glass interface (figure 2(b)), we need to concretize the parameters of the defect ensemble in a crystal–glass composite. In doing so, we consider a model two-phase crystal–glass composite under the following simplifying assumptions:

(i) Both the phases are elastically isotropic solids with the same values of the shear modulus μ and the same values of the Poisson ratio ν.

(ii) The amorphous phase contains wedge disclinations with straight lines normal to the crystal–glass interface (figure 3).

(iii) In spirit of the disclination models [29–32], the amorphous metallic phase is assumed to contain the two basic types of disclinations: large- and small-strength ones (figure 3). Each large-strength disclination is characterized by a negative strength ω_0 being around -0.5 rad. (The strength of disclination is equal here to the Frank pseudo-vector modulus if the disclination is associated with inserting an elastic wedge into the material and has the value opposite to the Frank pseudo-vector modulus if the disclination is associated with removing such a wedge.) The line of large-strength disclination changes the topology of elementary units (atomic clusters) adjacent to the line, compared to that of clusters composing the surrounding amorphous metallic material (for details, see [31, 32]). Small-strength disclinations are characterized by infinitesimal values of positive strength $\mathrm{d}\omega$. Their cores do not influence the topology of atomic clusters of glasses. Each large-strength (ω_0) disclination is surrounded by continuously and homogeneously distributed small-strength ($\mathrm{d}\omega$) disclinations which provide the complete screening of stress fields generated by the large-strength disclination. In doing so, small-strength disclinations are continuously distributed in the cylindrical region with nanoscale radius R_s and the centre line coinciding with the line of the large-strength disclination (figure 3). The sum strength of the negative disclination ω_0 and positive disclinations $\mathrm{d}\omega$ is supposed to equal to zero.

(iv) The large-strength disclinations are distributed in a tentatively homogeneous way within the amorphous phase. Their mean density is around R_s^{-2}. That is, the disclination ensemble of the glassy phase adjacent to the crystal–glass interface can be divided into

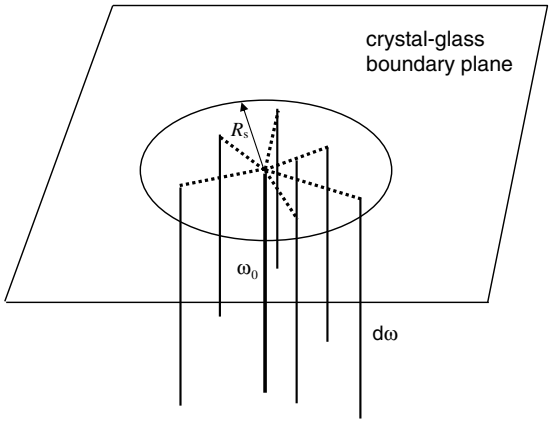

Figure 3. Large-strength ω_0-disclination (solid segment) of wedge type surrounded by continuously distributed dω-disclinations of wedge type in amorphous film on crystalline substrate. Some of the dω-disclinations are shown as straight segments. ω_0- and dω-disclinations are joined by twist disclination (dotted) segments in the crystal–glass interface plane. Wedge and twist disclinations form semiloops. R_s is the radius of the cylindrical region where the complete mutual screening of stress fields of ω_0- and dω-disclinations occurs.

disclination configurations with screened stress fields within nanoscale cylindrical regions which occupy all the glassy phase and do not overlap essentially.

The key structural and behavioral features of crystal–glass composites, reflected in their disclination description, are not oversimplified by using assumptions (i)–(iv). At the same time, these assumptions technically simplify our following analysis of crystal–glass interfaces. Notice that model assumption (iii) is concerned with the metallic glassy phase where continuously distributed disclinations of small negative strength surround isolated disclinations of large positive strength. Our consideration can be generalized to the case of other disclinated solids. For instance, in order to describe the covalent glass–crystal interfaces, we should reformulate assumption (iii) for the covalent glassy phase, taking into account that it contains both positive and negative large-strength isolated disclinations [30].

Let us consider the peculiarities of misfit disclination structures at the crystal–glass interface, with model assumptions (i)–(iv) taken into account. In the situation discussed, the wedge disclinations of the metallic glassy phase terminate at the crystal–glass interface where they transform into twist disclinations (figure 3). The twist disclinations located at the crystal–glass interface join termination points of wedge disclinations in accordance with the disclination charge (Frank pseudo-vector) conservation law (figure 3). In the framework of our model, the disclination ensemble of the glassy phase adjacent to the crystal–glass interface can be divided into disclination configurations with screened stress fields within cylindrical regions (figure 3). Within each such region a large negative-strength (ω_0) wedge disclination is surrounded by continuously distributed small positive-strength (dω) wedge disclinations.

For the convenience of the following calculations, we treat the disclination with the large negative strength ω_0 as an ensemble of small-negative-strength disclinations, each having the strength $-$dω. All the small-negative-strength disclinations have the lines coinciding with the line of the large-strength disclination. Their sum strength is equal to ω_0. In this context, the sum strength of negative ($-$dω) and positive (dω) disclinations with small strengths is zero, and the distribution density of disclinations having the strength $-$dω equals to that of disclinations having the strength dω. Therefore, the negative disclination with the large strength ω_0 and the

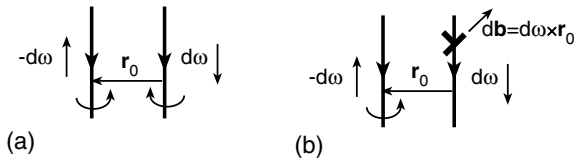

Figure 4. Two-axis dipole of disclinations with the strengths $\mathrm{d}\omega$ and $-\mathrm{d}\omega$ (a) is equivalent to a one-axis disclination dipole and a dislocation with the Burgers vector $\mathrm{d}\boldsymbol{b}$, whose line coincides with that of the of the disclination with the strength $\mathrm{d}\omega$.

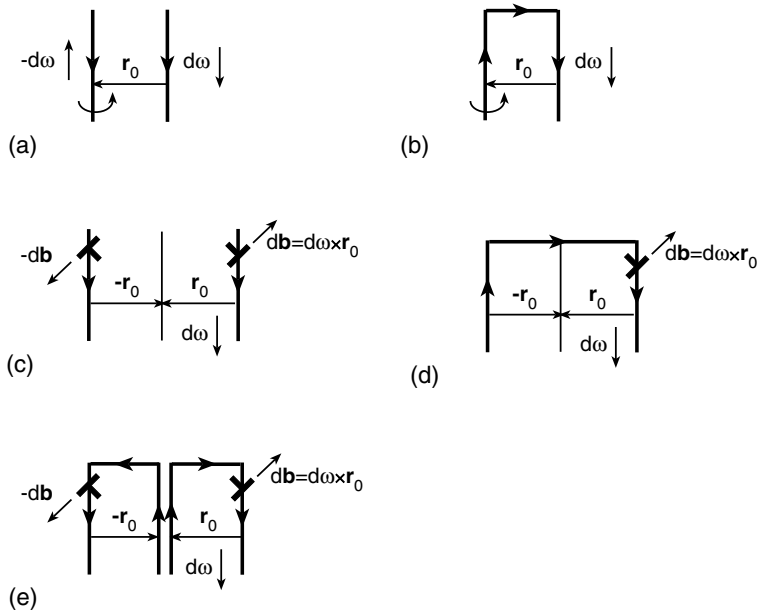

Figure 5. Transformations of defect configurations. Transformation of (a) one-axis disclination dipole into (b) disclination semiloop. Transformation of (c) dislocation dipole into (d) dislocation semiloop being equivalent to (e) the superposition of two dislocation semiloops.

ensemble of positive disclinations having the strength $\mathrm{d}\omega$ can be represented as an ensemble of dipoles of disclinations $\mathrm{d}\omega$ and $-\mathrm{d}\omega$. The disclinations $\mathrm{d}\omega$ stand off the axis of the cylindrical region occupied by the disclinations while all the negative disclinations $-\mathrm{d}\omega$ are located at the cylinder axis.

Any dipole of disclinations $\mathrm{d}\omega$ and $-\mathrm{d}\omega$ has two rotation axes. According to the theory of disclinations [31, 39], any dipole of disclinations $\mathrm{d}\omega$ and $-\mathrm{d}\omega$ with two rotation axes (that coincide with the disclination lines) can be presented as the superposition of the two following defects: (i) disclination dipole with one rotation axis that is coincident with the cylinder centre line and (ii) dislocation whose line coincides with the line of the disclination $\mathrm{d}\omega$, and the Burgers vector $\mathrm{d}\boldsymbol{b}$ follows as $\mathrm{d}\boldsymbol{b} = \mathrm{d}\boldsymbol{\omega} \times r_0$. Here $\mathrm{d}\boldsymbol{\omega}$ denotes the disclination Frank pseudo-vector, and $\boldsymbol{r}_0$ is the vector that characterizes the displacement of the disclination rotation axis (from one wedge disclination to the other) (figure 4). Similarly to the disclinations, the lines of dislocations are homogeneously distributed within the cylindrical region of radius R_s.

In accordance with the Frank conservation law, the disclinations that comprise one-axis dipoles (figure 5(a)) are closed to form disclination semiloops (figure 5(b)) by twist disclination segments of strength $\mathrm{d}\omega$ (located at the crystal–glass interface). According to the conservation

law of the Burgers vector, the dislocation lines that occupy the cylindrical region of radius R_s also have to be closed into semiloops. To join the dislocation lines, consider two dislocations that are characterized by opposite vectors $\boldsymbol{r}_0$ and $-\boldsymbol{r}_0$ (and so have opposite Burgers vectors $\mathrm{d}\boldsymbol{\omega} \times \boldsymbol{r}_0$ and $-\mathrm{d}\boldsymbol{\omega} \times \boldsymbol{r}_0$) (figure 5(c)). These dislocations may be closed into a semiloop (figure 5(d)) by an edge dislocation segment (located at the crystal–glass interface). In turn, the dislocation semiloop thus formed may be presented as the superposition of two dislocation semiloops shown in figure 5(e). Evidently, the positions and directions of the lines of dislocation semiloops shown in figure 5(e) coincide with those of the disclination semiloops characterized by the vectors r_0 and $-r_0$ (see figure 5(b)). Therefore, the combination of two semiloops (disclination and dislocation ones) with the same lines may be considered as one disclination–dislocation semiloop, or Volterra dislocation, characterized by the Frank pseudovector $\mathrm{d}\boldsymbol{\omega}$ and the Burgers vector $\mathrm{d}\boldsymbol{b} = \mathrm{d}\boldsymbol{\omega} \times \boldsymbol{r}_0$.

To summarize, in the framework of our model, the defect configuration within the cylindrical region in the glassy phase adjacent to the crystal–glass interface can be effectively represented as the superposition of Π-like disclination–dislocation semiloops. Each Π-like semiloop consists of (a) a segment located at the cylinder centre line normal to the crystal–glass interface; (b) a segment normal to the crystal–glass interface and standing off the cylinder axis; and (c) a segment of length r_0, which is located at the crystal–glass interface and joins segments (a) and (b).

4. Stress fields of disclination–dislocation loops in crystal–glass composite

In order to estimate the elastic energy of a crystal–glass interface, we need to calculate the stress field of the disclination–dislocation ensemble in a composite solid containing the interface. The stress fields created by the ensemble of dislocation–disclination semiloops continuously distributed over a cylindrical region is effectively calculated using the method based on representations of the ensemble of the defect semiloops as a cylindrical inclusion with a certain plastic distortion (figure 6); for details, see the appendix. With the results of our calculations presented in the appendix, we find the stress tensor components written in the cylindrical coordinates (r, φ, z) (see figure 6) to be as follows: $\sigma_{jl} = \sigma^{\infty}_{jl}\Theta(\tilde{z}) + \sigma'_{jl}\,\mathrm{sgn}\,\tilde{z}$, where

$$\sigma^{\infty}_{rr} = -\frac{D\omega_0}{4}\left\{(\tilde{r}^2 - 4\ln\tilde{r})\Theta(1-\tilde{r}) + \frac{1}{\tilde{r}^2}\Theta(\tilde{r}-1)\right\}, \tag{1a}$$

$$\sigma^{\infty}_{\varphi\varphi} = -\frac{D\omega_0}{4}\left\{(3\tilde{r}^2 - 4\ln\tilde{r} - 4)\Theta(1-\tilde{r}) - \frac{1}{\tilde{r}^2}\Theta(\tilde{r}-1)\right\}, \tag{1b}$$

$$\sigma^{\infty}_{zz} = -\nu D\omega_0(\tilde{r}^2 - 2\ln\tilde{r} - 1)\Theta(1-\tilde{r}), \tag{1c}$$

$$\sigma^{\infty}_{r\varphi} = \sigma^{\infty}_{rz} = \sigma^{\infty}_{z\varphi} = 0, \tag{1d}$$

$$\sigma'_{\{\substack{rr\\ \varphi\varphi}\}} = \frac{D\omega_0}{24}\int_0^{\infty} \mathrm{e}^{-k|\tilde{z}|}k\,\mathrm{d}k\,\{[(k|\tilde{z}| - 4(1-\nu))J_0(k\tilde{r}) \mp (k|\tilde{z}| - 2)J_2(k\tilde{r})]f_1(k) + [(k|\tilde{z}| - 2)J_0(k\tilde{r}) \mp (k|\tilde{z}| - 2(1-2\nu))J_2(k\tilde{r})]f_2(k)\}, \tag{2a}$$

$$\sigma'_{zz} = -\frac{D\omega_0}{12}\int_0^{\infty} J_0(k\tilde{r})\mathrm{e}^{-k|\tilde{z}|}k\,\mathrm{d}k\,\{k|\tilde{z}|[f_1(k) + f_2(k)] - 2\nu[f_1(k) - f_2(k)]\}, \tag{2b}$$

$$\sigma'_{rz} = -\frac{D\omega_0}{12}\int_0^{\infty} J_1(k\tilde{r})\mathrm{e}^{-k|\tilde{z}|}k\,\mathrm{d}k\,\{k|\tilde{z}|[f_1(k) + f_2(k)] - 2(1-\nu)f_1(k) - (1-2\nu)f_2(k)\}, \tag{2c}$$

$$\sigma'_{r\varphi} = \sigma'_{z\varphi} = 0, \tag{2d}$$

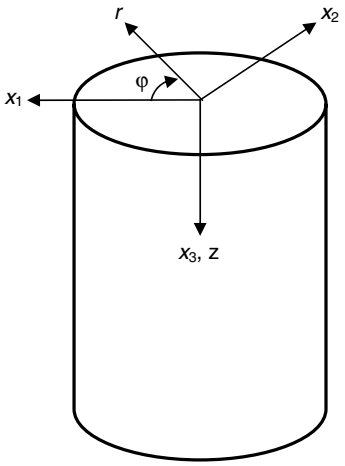

Figure 6. Cylindrical inclusion that is equivalent to an ensemble of dislocation–disclination semiloops and its associated coordinate systems.

$\tilde{r} = r/R_s$, $\tilde{z} = z/R_s$, and $D = \mu/[2\pi(1-\nu)]$. Here $\Theta(t)$ is the Heaviside function equal to 1, if $t > 0$, and to 0, if $t < 0$, $J_n(k\tilde{r})$ are the Bessel functions of the mth order, and the functions $f_1(k)$ and $f_2(k)$ are given by formulae (A.21) and (A.22). The stress tensor components σ_{jl} given by formulae (1) and (2) satisfy the equilibrium equations: $\sigma_{jl,l} = 0$. Also, from formulae (1) and (2) it follows that $\sigma_{jl}^{\infty} = \lim_{z\to+\infty} \sigma_{jl}$. In these circumstances, the stresses σ_{jl}^{∞} represent the stresses created in an infinite amorphous solid by the ensemble of two-axis disclination dipoles continuously distributed over a cylindrical region with the radius R_s. The stresses σ'_{jl} are the stresses occurring owing to the presence of the crystal–glass boundary. They exist only in the vicinity of this interphase boundary and quickly decay with increasing distance from this boundary (for an illustration, see figure 7). Due to the stresses σ'_{jl}, the elastic energy density (per unit volume) in a local region adjacent to the boundary and thereby the total elastic energy of a crystal–glass composite increase. Since the stresses σ'_{jl} are associated with the existence of the crystal–glass boundary, their contribution to the total energy of a crystal–glass composite solid is naturally treated as the elastic energy of the boundary. This energy will be calculated in the next section.

5. Elastic energy of crystal–glass interphase boundary

Let us consider the elastic energy W accumulated in a crystal–glass composite solid owing to the presence of dislocation–disclination semiloops continuously distributed over a cylindrical region with radius R_s. Following the general approach [40], the energy W can be written in the following form:

$$W = -\tfrac{1}{2}\int_{V_{cg}} \sigma_{jl}\beta_{lj}^{*}\,\mathrm{d}V, \tag{3}$$

where V_{cg} is the volume of the crystal–glass composite and β_{lj}^{*} is the total plastic distortion of the ensemble of dislocation–disclination semiloops. In the cylindrical coordinate system (r, φ, z), β_{lj}^{*} has only one non-zero component $\beta_{\varphi\varphi}^{*}$, given by formula (A.11). Since $\sigma_{jl} = \sigma_{jl}^{\infty}\Theta(\tilde{z}) + \sigma'_{jl}\operatorname{sgn}\tilde{z}$ (where $\tilde{z} > 0$ in the amorphous phase, and $\tilde{z} < 0$ in the crystal phase) and $\beta_{lj}^{*} = 0$ at $\tilde{z} < 0$ (in the crystal phase), formula (3) can be represented as: $W = W_0 + W_i$, where

$$W_0 = -\tfrac{1}{2}\int_{V_g} \sigma_{jl}^{\infty}\beta_{lj}^{*}\,\mathrm{d}V, \qquad W_i = -\tfrac{1}{2}\int_{V_g} \sigma'_{jl}\beta_{lj}^{*}\,\mathrm{d}V, \tag{4}$$

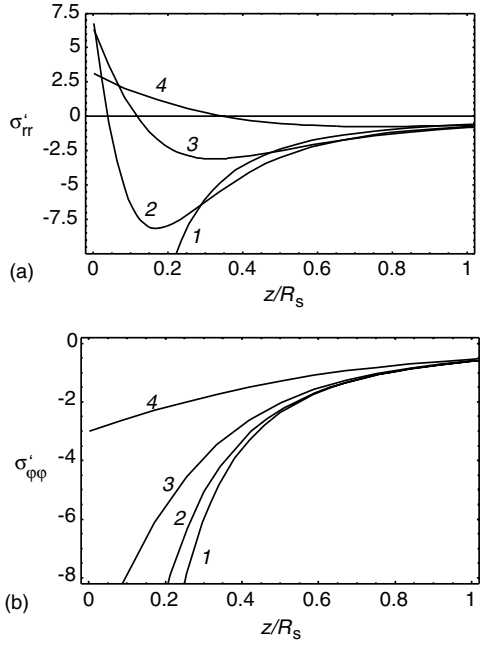

Figure 7. Dependences of the stresses σ'_{rr} (a) and $\sigma'_{\varphi\varphi}$ (b) on the dimensionless distance z/R_s from the crystal–glass interface, for $r/R_s = 0$, 0.3, 0.5, 1 (curves 1, 2, 3 and 4, respectively).

and V_g is the volume occupied by the amorphous phase. In doing so, W_0 is the elastic energy of the ensemble of two-axis disclination dipoles (distributed over the cylindrical region with the radius R_s) in the volume V_g of infinite amorphous material. W_i plays the role of the additional energy related to the transformation of the two-axis disclination dipoles into the dislocation–disclination semiloops at the crystal–glass boundary. Since the tensor β^*_{lj} in the cylindrical coordinate system has the only one non-zero component $\beta^*_{\varphi\varphi}$, the second expression in formula (4) can be represented as

$$W_i = -\tfrac{1}{2}\int_0^\infty r\,\mathrm{d}r \int_0^{2\pi} \mathrm{d}\varphi \int_0^\infty \mathrm{d}z\,\sigma'_{\varphi\varphi}\beta^*_{\varphi\varphi}. \tag{5}$$

Substitution of expressions (A.11) and (2*a*) for $\beta^*_{\varphi\varphi}$ and $\sigma'_{\varphi\varphi}$ into formula (5) and subsequent integration yield

$$W_i = \frac{D\omega_0^2 R_s^3}{144}\left\{(1+4\nu)A + 2B + (1-4\nu)C\right\}, \tag{6}$$

where

$$A = \int_0^\infty f_1^2(k)\,\mathrm{d}k \approx 2.76, \qquad B = \int_0^\infty f_1(k)\,f_2(k)\,\mathrm{d}k \approx 0.72,$$
$$C = \int_0^\infty f_2^2(k)\,\mathrm{d}k \approx 0.44, \tag{7}$$

and the functions $f_1(k)$ and $f_2(k)$ are given by (A.20) and (A.21), as above.

As noted above, the energy W_i is treated as the energy of the crystal–glass boundary, related to the presence of dislocation–disclination semiloops continuously distributed over one cylindrical region with the radius R_s. In the framework of our model (see section 3), such cylindrical regions with dislocation–disclination semiloop ensembles occupy all the amorphous phase (except for some small areas between the cylindrical regions, which are free from defects and assumed to be incoherent), and their stress fields do not interact. In this

model approximation, the energy density $\gamma_{\rm i}$ of the interphase crystal–glass boundary per its unit area is defined as the ratio of W_i to the cylindrical section area with the radius $R_{\rm s}$, that is, $\gamma_{\rm i} = W_i/(\pi R_{\rm s}^2)$. With (6), we find

$$\gamma_{\rm i} = \frac{D\omega_0^2 R_{\rm s}}{144\pi}\{(1+4\nu)A + 2B + (1-4\nu)C\}. \tag{8}$$

For polyatomic metallic glasses (amorphous metallic alloys), we have [31, 32] $\omega \approx -0.5$ and $R_{\rm s} \approx 5a_0$ (where a_0 is the mean interatomic distance in the glassy phase, and $R_{\rm s}$ is treated to be tentatively equal to the characteristic length scale of structural inhomogeneities in amorphous metallic alloys [41]). In this case, for $\nu = 0.3$, from formula (8), we find an estimate of $\gamma_{\rm i}/(\mu a_0) \approx 0.47 \times 10^{-2}$. For monatomic metallic glasses (amorphous metals), $\omega_0 = -2\arcsin(1/\sqrt{3}) \approx -70.5^\circ$, $R_{\rm s} \approx 5a_0$ [31, 32]. In this case, for $\nu = 0.3$, from formula (8) we find estimate of $\gamma_{\rm i}/(\mu a_0) \approx 2.82 \times 10^{-2}$. The above estimated values of the energy density $\gamma_{\rm i}$ that characterizes the crystal–glass boundary are close to values of the chemical energy density that characterize crystal–crystal interphase boundaries and free surfaces of crystalline solids. For instance, from data [42, 43] on materials parameters for Cu and Ni, we have the following estimates: for Cu $\gamma/(\mu a_0) = (11\text{–}18) \times 10^{-2}$, $\gamma_b/(\mu a_0) = (7\text{–}10) \times 10^{-2}$, for Ni $\gamma/(\mu a_0) = (8\text{–}14) \times 10^{-2}$, $\gamma_b/(\mu a_0) = (7\text{–}9) \times 10^{-2}$. Here γ and γ_b denote the surface and grain boundary energies, respectively. Thus, values of γ and γ_b are of the same order as the elastic energy density $\gamma_{\rm i}$ of a crystal–glass boundary.

In the situation where the crystal and amorphous phases in a crystal–glass composite solid have the same chemical composition, the total energy density of the crystal–glass interface is equal to the elastic energy density $\gamma_{\rm i}$. If the adjacent crystal and amorphous phases have different chemical compositions A and B, respectively, the total energy of the interface between the crystal A and glass B is represented in the first approximation as the sum $\gamma_{\rm i} + \gamma_{\rm AB}$, where $\gamma_{\rm AB}$ is the chemical energy density that characterizes the interphase boundary between the crystals A and B.

6. Concluding remarks

Here we have suggested a first approximation model that describes misfit defects at crystal–glass interfaces in composite solids. In the framework of the suggested model, crystal–glass interfaces are effectively described as semi-coherent interfaces with high-density ensembles of misfit disclinations. Such disclinations are associated with orientational misfit between the adjacent glassy phase (characterized by a short-range orientational order) and the crystalline phase (characterized by a long-range orientational order). The misfit stresses in amorphous films are treated as generated by crystal–glass interfaces due to the existence of misfit disclinations and the difference between the mean interatomic distance of the amorphous phase and the lattice parameter of the crystalline phase. With the model representations elaborated in this paper, we have calculated the characteristics (in particular, the elastic energy density) of crystal–glass interfaces. Following our quantitative examinations, the elastic energy density of the crystal–glass interfaces can be rather high and is highly sensitive to the characteristics (the disclination strength ω_0, the screening length $R_{\rm s}$ of disclination stress fields) of the disclination ensemble in the film.

The quantitative results obtained in this paper are approximate. However, they can be used as a basis for further, more detailed investigations of crystal–glass composites. In particular, the calculated values of the elastic energy density of crystal–glass interfaces can be used as an input in a theoretical analysis of solid state amorphizing transformations under thermal, irradiation and mechanical treatments as well as adhesion failure processes in amorphous films on crystalline substrates. This will be the subject of our further investigations.

Acknowledgments

This work was supported, in part, by the Russian Fund of Basic Research (grant 04-01-00211) (for SVB); by INTAS (grant 03-51-3779), Russian Academy of Sciences programme 'Structural mechanics of materials and construction elements' and St Petersburg Scientific Centre (for SVB, IAO and AGS); by the Office of US Naval Research (grant N00014-01-1-1020) and the Russian Science Support Foundation (for IAO); and by the Physics of Solid State Nanostructures Programme of the Ministry of Industry and Science of Russia (for AER).

Appendix

In this appendix, we calculate the stress field of the ensemble of dislocation–disclination semiloops (figure 3) continuously distributed over a semi-infinite cylindrical region. In the cylindrical coordinate system shown in figure 6, this region occupies the domain ($r < R_s$, $z > 0$). To calculate the stress field of the dislocation–disclination ensemble, we present it as a cylindrical inclusion whose plastic distortion is equal to the total plastic distortion of the ensemble of the dislocation–disclination semiloops.

In spirit of the general approach [44], the total distortion (gradient of the displacement field) $u_{i,j}$ created by the defect configuration under consideration (figure 3) can be represented as the sum of elastic distortion β_{ji} and plastic distortion β^*_{ji}:

$$u_{i,j} = \beta_{ji} + \beta^*_{ji}. \tag{A.1}$$

The elastic distortion tensor β_{ji} is in the following relationship [40] with the tensor of elastic stresses σ_{ij}:

$$\sigma_{ij} = C_{ijkl}\beta_{lk}, \tag{A.2}$$

where C_{ijkl} is the tensor of elastic moduli.

Let us consider a dislocation–disclination (semi)loop which represents a superposition of dislocation (semi)loop with the Burgers vector $\boldsymbol{b}$ and disclination (semi)loop with the Frank pseudo-vector $\boldsymbol{\omega}$. The dislocation–disclination (semi)loop or, in other terms, Volterra dislocation can be treated as the defect resulting from the following imaginary operation. A solid is cut along surface S, in which case two free surfaces S^+ and S^- are formed at the cut surface S. The free surface S^+ moves (translates and rotates) by the vector $\boldsymbol{u}(\boldsymbol{x}) = \boldsymbol{b} + \omega \times (\boldsymbol{x} - \boldsymbol{x}^0)$ relative to the free surface S^-, where $\boldsymbol{x} = (x_1, x_2, x_3)$ is an arbitrary three-dimensional vector, and $\boldsymbol{x}^0$ is the vector that describes both the spatial position and orientation of the rotation axis. The Volterra dislocation line and the surfaces S^+ and S^- are in the relationship given by the following rule: go around a linking circuit (the Burgers or Frank circuit) in the direction of rotation of a right-handed screw advancing along the direction of the dislocation. Then the surface S^+ is designated as the surface at which the end point of the Burgers (Frank) circuit is located.

The plastic distortion β^{*l}_{ij} of the dislocation–disclination (semi)loop under consideration is given as [40]

$$\beta^{*l}_{ij} = \delta_S(S)[-b_j - e_{jpq}\omega_p(x_q - x^0_q)]n_i, \tag{A.3}$$

where $\delta_S(S) = \int_S \delta(\boldsymbol{x} - \boldsymbol{x}')\,\mathrm{d}S'$, $\delta(\boldsymbol{x} - \boldsymbol{x}')$ is the three-dimensional delta-function, n_i is the vector normal to S and directed from S^+ to S^-, e_{jpq} is the permutation tensor.

Now let us consider a dislocation–disclination semiloop consisting of disclination and dislocation semiloops characterized by an infinitesimal Frank pseudo-vector $\mathrm{d}\boldsymbol{\omega}$ and the Burgers vector $\mathrm{d}\boldsymbol{b} = \mathrm{d}\boldsymbol{\omega} \times \boldsymbol{r}_0$, respectively (figure A.1). For our consideration, let us introduce the two Cartesian coordinate systems: (x_1, x_2, x_3) and (x'_1, x'_2, x'_3). The axes x_3 and x'_3 coincide,

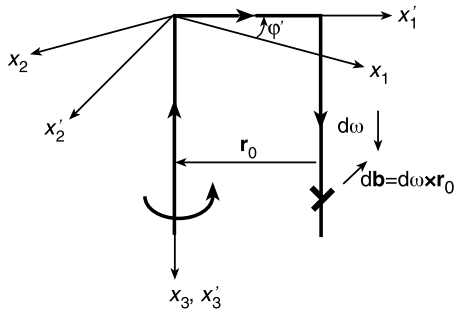

Figure A.1. Two Cartesian coordinate systems (x_1, x_2, x_3) and (x_1', x_2', x_3') characterize the spatial position of the disclination–dislocation semiloop.

while the axes x_1' and x_2' result from the axes x_1 and x_2 respectively by their anticlockwise rotation by φ' in the plane $0x_1x_2$. Also, the axis x_1' lies in the semiloop plane, and the direction of the semiloop line is chosen as shown in figure A.1. In this situation, the Frank pseudo-vector $\mathrm{d}\boldsymbol{\omega} = \mathrm{d}\omega\, \boldsymbol{e}_{x_3'}$ of the defect semiloop is directed along the axis x_3', while the direction of its Burgers vector is opposite to that of the axis x_2': $\mathrm{d}\boldsymbol{b} = -\mathrm{d}\omega\, r_0 \boldsymbol{e}_{x_2'}$. The rotation axis that characterizes the dislocation–disclination semiloop coincides with the axis x_3'.

The plastic distortion $\mathrm{d}\beta_{ij}^*$ of the defect semiloop under consideration can be calculated using formula (A.3). In doing so, we find that the tensor $\mathrm{d}\beta_{ij}^*$ in the coordinate system (x_1', x_2', x_3') has the two following non-zero components:

$$\mathrm{d}\beta_{2'2'}^* = \mathrm{d}\omega\, \delta(x_2')[\Theta(r_0 - x_1') - \Theta(-x_1')]\Theta(x_3')(x_1' - r_0), \tag{A.4}$$

$$\mathrm{d}\beta_{2'1'}^* = -\mathrm{d}\omega\, x_2'\delta(x_2')[\Theta(r_0 - x_1') - \Theta(-x_1')]\Theta(x_3'). \tag{A.5}$$

Here $\Theta(t)$ is the Heaviside function equal to 1, if $t > 0$, and to 0, if $t < 0$.

Let us introduce the cylindrical coordinates r, φ and z related to the coordinates x_1, x_2 and x_3 by the following relationships: $x_1 = r\cos\varphi$, $x_2 = r\sin\varphi$, $x_3 = z$ (see figure 6). Then we have $x_1' = r\cos(\varphi - \varphi')$, $x_2' = r\sin(\varphi - \varphi')$. Using the latter relations, formulae (A.4) and (A.5) and standard transformations of tensor components at rotations of the coordinate system, the non-zero components of the tensor $\mathrm{d}\beta_{ij}^*$ are written in the coordinate system (x_1, x_2, x_3) as follows:

$$\mathrm{d}\beta_{11}^* = A(r, r_0, \varphi - \varphi')(r\sin\varphi - r_0\sin\varphi')\sin\varphi', \tag{A.6}$$

$$\mathrm{d}\beta_{22}^* = A(r, r_0, \varphi - \varphi')(r\cos\varphi - r_0\cos\varphi')\cos\varphi', \tag{A.7}$$

$$\mathrm{d}\beta_{12}^* = A(r, r_0, \varphi - \varphi')(-r\cos\varphi + r_0\cos\varphi')\sin\varphi', \tag{A.8}$$

$$\mathrm{d}\beta_{21}^* = A(r, r_0, \varphi - \varphi')(-r\sin\varphi + r_0\sin\varphi')\cos\varphi', \tag{A.9}$$

where

$$A(r, r_0, \varphi - \varphi') = \mathrm{d}\omega\{\Theta[r_0 - r\cos(\varphi - \varphi')] - \Theta[-r\cos(\varphi - \varphi')]\}\delta[r\sin(\varphi - \varphi')]\Theta(z). \tag{A.10}$$

Now let us turn to analysis of continuous distributions of dislocation–disclination semiloops existing in a crystal–glass composite. Let us consider the situation where one of the segments of dislocation–disclination semiloops is located at line $z = 0$, and the semiloops are continuously distributed over a cylinder with the radius R_s in the half-space $z \geqslant 0$ occupied by the amorphous phase. The distribution of the semiloops is parametrized by the coordinates $r = r_0$ and $\varphi = \varphi'$ of their segments parallel to the axis z, and is homogeneous within the cylinder. In this situation, the magnitude $\mathrm{d}\omega$ of the infinitesimal disclination Frank pseudo-vector is given by the relationship $\mathrm{d}\omega = -[\omega_0/(\pi R_s^2)]r_0\,\mathrm{d}r_0\,\mathrm{d}\varphi'$, and the total distortion of the ensemble of the continuously distributed defect semiloops is

$\beta^*_{ij} = \int_{r<R_s} \mathrm{d}\beta^*_{ij}$. This integral, with formulae (A.6)–(A.10), yields: $\beta^*_{11} = \beta^*_{\varphi\varphi}\sin^2\varphi$, $\beta_{22} = \beta^*_{\varphi\varphi}\cos^2\varphi$, $\beta^*_{12} = \beta^*_{21} = -\beta^*_{\varphi\varphi}\sin\varphi\cos\varphi$, where

$$\beta^*_{\varphi\varphi} = \frac{\omega_0}{6\pi}\frac{\tilde{r}^3 - 3\tilde{r} + 2}{\tilde{r}}\Theta(1-\tilde{r})\Theta(\tilde{z}), \tag{A.11}$$

$\tilde{r} = r/R_s$, and $\tilde{z} = z/R_s$. It is evident that $\beta^*_{\varphi\varphi}$ is the sole non-zero component of the total plastic distortion tensor β^*_{ij} in the cylindrical coordinate system (r, φ, z).

With the above expressions for the plastic distortion β^*_{ij} of the ensemble of continuously distributed dislocation–disclination semiloops, let us calculate the stress field created by this ensemble. Following the general approach [40], the plastic distortion β^*_{ij} induces the displacement field given in its general form as

$$u_p(\boldsymbol{x}) = \frac{1}{(2\pi)^3}\int_{V_k} \hat{u}_p(\boldsymbol{k})\mathrm{e}^{\mathrm{i}\boldsymbol{k}\cdot\boldsymbol{x}}\,\mathrm{d}V'_k, \tag{A.12}$$

where

$$\hat{u}_p(\boldsymbol{k}) = -\mathrm{i}k_l C_{jlmn}\hat{\beta}^*_{nm}\hat{G}_{pj}. \tag{A.13}$$

In formulae (A.12) and (A.13), $\mathrm{i} = \sqrt{-1}$, $\hat{u}_p$, $\hat{\beta}^*_{nm}$ and $\hat{G}_{pj}$ are the Fourier transforms of the plastic distortion tensor and Green tensor of the medium, respectively, $\mathrm{d}V'_k$ is an elemental volume in reciprocal (Fourier) space, $\boldsymbol{x}$ and $\boldsymbol{k}$ are the three-dimensional vectors in conventional and reciprocal (Fourier) spaces, respectively, and $\boldsymbol{k}\cdot\boldsymbol{x}$ is their scalar product. Integration in formula (A.12) is performed over the infinite volume V_k of the Fourier space.

In the case of an isotropic medium, we have [40]

$$C_{jlmn} = \lambda\delta_{jl}\delta_{mn} + \mu(\delta_{jm}\delta_{ln} + \delta_{jn}\delta_{lm}), \tag{A.14}$$

$$\hat{G}_{ij} = \frac{(\lambda+2\mu)k^2\delta_{ij} - (\lambda+\mu)k_i k_j}{\mu(\lambda+2\mu)k^4}. \tag{A.15}$$

Here $\lambda = 2\nu\mu/(1-2\nu)$, $k^2 = \boldsymbol{k}\cdot\boldsymbol{k}$, and δ_{ij} is the Kronecker symbol.

Let us introduce the cylindrical coordinate system $(k_\parallel,\ \psi,\ k_z)$ into the Fourier space (figure A.2). The magnitudes $k_\parallel$, ψ and k_z are in the following relationships with the projections k_1, k_2 and k_3 of the vector $\boldsymbol{k}$ on the axes x_1, x_2 and x_3, respectively: $k_1 = k_\parallel\cos\psi, k_2 = k_\parallel\sin\psi$, $k_3 = k_z$. $k_\parallel$ is the magnitude of the vector $\boldsymbol{k}_\parallel$, which represents the projection of the vector $\boldsymbol{k}$ onto the plane $0x_1x_2$ and makes the angle ψ with the axis x_1. Since the projection $\boldsymbol{r}$ of the vector $\boldsymbol{x}$ on the same plane makes the angle φ with the axis x_1, the angle between the vectors $\boldsymbol{k}_\parallel$ and $\boldsymbol{r}$ is $\pm(\psi-\varphi)$. As a corollary, we have $\boldsymbol{k}\cdot\boldsymbol{x} = k_\parallel r\cos(\psi-\varphi) + k_z z$. With this relationship, the Fourier image $\hat{\beta}^*_{ij}$ of the plastic distortion tensor β^*_{ij} is written as

$$\hat{\beta}^*_{ij} = \int_0^\infty r\,\mathrm{d}r\int_0^{2\pi}\mathrm{d}\varphi\int_{-\infty}^{\infty}\mathrm{d}z\,\beta^*_{ij}\mathrm{e}^{-\mathrm{i}(k_\parallel r\cos(\psi-\varphi)+k_z z)}. \tag{A.16}$$

Substitution of expressions for the tensor β^*_{ij} components into formula (A.16) yields

$$\hat{\beta}^*_{11} = \hat{\beta}^*_1 + \hat{\beta}^*_2\cos 2\psi, \qquad \hat{\beta}^*_{22} = \hat{\beta}^*_1 - \hat{\beta}^*_2\cos 2\psi, \qquad \hat{\beta}^*_{12} = \hat{\beta}^*_{21} = \hat{\beta}^*_2\sin 2\psi, \tag{A.17}$$

where

$$\hat{\beta}^*_1 = \frac{\omega_0 R_s^3}{6}f_1(k_\parallel R_s)\left(\pi\delta(k_z R_s) + \frac{1}{\mathrm{i}k_z R_s}\right), \tag{A.18}$$

$$\hat{\beta}^*_2 = \frac{\omega_0 R_s^3}{6}f_2(k_\parallel R_s)\left(\pi\delta(k_z R_s) + \frac{1}{\mathrm{i}k_z R_s}\right), \tag{A.19}$$

$$f_1(k) = -\frac{2[kJ_1(k) + J_2(k)]}{k^2} + 2{}_1F_2(1/2;\,1,\,3/2;\,-k^2/4), \tag{A.20}$$

$$f_2(k) = \frac{2[k(J_0(k)-3) + (k^2+4)J_1(k)]}{k^3} + \frac{k^2}{12}{}_1F_2(3/2;\,5/2,\,3;\,-k^2/4). \tag{A.21}$$

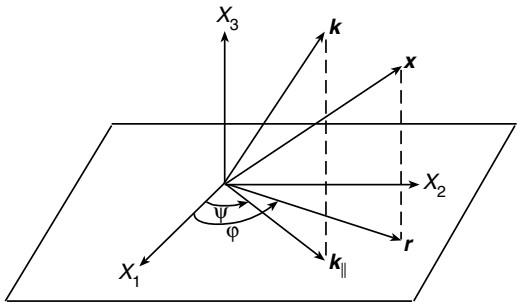

Figure A.2. Spatial positions of vectors $\boldsymbol{k}$ and $\boldsymbol{x}$.

In formulae (A.20) and (A.21), $J_m(x)$ are the Bessel functions of the mth order, and ${}_1F_2(a_1; b_1, b_2; t)$ are the generalized hypergeometric series given as [45]

$$ {}_1F_2(a_1; b_1, b_2; t) = \frac{\Gamma(b_1)\Gamma(b_2)}{\Gamma(a_1)} \sum_{n=0}^{\infty} \frac{\Gamma(a_1+n)}{\Gamma(b_1+n)\Gamma(b_2+n)} \frac{x^n}{n!}, \tag{A.22} $$

with $\Gamma(x)$ being the gamma-function.

Thus, we have all the terms figuring in formula (A.13) for the Fourier image $\hat{u}_{\mathrm{p}}(\boldsymbol{k})$ of the displacement field created by the ensemble of continuously distributed dislocation–disclination semiloops. This allows us to calculate the Fourier image $\hat{\sigma}_{jl}(\boldsymbol{k})$ of the elastic stress field created by the ensemble in question. As follows from formulae (A.1) and (A.2),

$$ \sigma_{jl} = C_{jlmn}(u_{m,n} - \beta^*_{nm}). \tag{A.23} $$

As a corollary, we have

$$ \hat{\sigma}_{jl} = C_{jlmn}(\mathrm{i}k_n\hat{u}_m - \hat{\beta}^*_{nm}). \tag{A.24} $$

With (A.13)–(A.15) and (A.17)–(A.19) substituted into formula (A.24), we find

$$ \begin{aligned} \hat{\sigma}_{jl} = \frac{\mu\omega_0 R_{\mathrm{s}}^3}{3(\lambda+2\mu)k^2}\left(\pi\delta(k_z R_{\mathrm{s}}) + \frac{1}{\mathrm{i}k_z R_{\mathrm{s}}}\right)\Bigg\{ & f_1(k_\parallel R_{\mathrm{s}})\Bigg[2(\lambda+\mu)\left(\frac{k_j k_l(k^2+k_z^2)}{k^2} - k^2\delta_{jl}\right) \\ & - (\lambda+2\mu)(k_3(k_j\delta_{l3} + k_l\delta_{j3}) - k^2\delta_{j3}\delta_{l3}) - \lambda k_3^2\delta_{jl}\Bigg] \\ & + f_2(k_\parallel R_{\mathrm{s}})\Bigg[(\lambda+2\mu)(2k_j k_l - k_3(k_j\delta_{l3} + k_l\delta_{j3}) - k^2((\delta_{j1}\delta_{l1} - \delta_{j2}\delta_{l2})\cos 2\psi \\ & + (\delta_{j1}\delta_{l2} + \delta_{j2}\delta_{l1})\sin 2\psi)) + \lambda k_\parallel^2\delta_{jl} - \frac{2(\lambda+\mu)k_j k_l k_\parallel^2}{k^2}\Bigg]\Bigg\}. \end{aligned} \tag{A.25} $$

The stress field σ_{jl} in a real space is derived from $\hat{\sigma}_{jl}$ (given by formula (A.25)), using the reverse Fourier transform, which in the cylindrical coordinates $(k_\parallel, \psi, k_z)$ has the following form:

$$ \sigma_{jl} = \frac{1}{(2\pi)^3}\int_0^\infty k_\parallel \,\mathrm{d}k_\parallel \int_0^{2\pi} \mathrm{e}^{\mathrm{i}k_\parallel r\cos(\psi-\varphi)}\,\mathrm{d}\psi \int_{-\infty}^{\infty} \hat{\sigma}_{jl}\mathrm{e}^{\mathrm{i}k_z z}\,\mathrm{d}k_z. \tag{A.26} $$

After integration in formula (A.26) and transformation of the expression for σ_{jl} from the Cartesian coordinate system (x_1, x_2, x_3) into the cylindrical coordinate system (r, φ, z), we come to the relation $\sigma_{jl} = \sigma_{jl}^{\infty}\Theta(\tilde{z}) + \sigma'_{jl}\,\mathrm{sgn}\,\tilde{z}$, where σ_{jl}^{∞} and σ'_{jl} are given by formulae (1) and (2).

References

[1] Zhao D Q, Pan M X, Wang W H, Wei B C, Okada T and Utsumi W 2003 *J. Phys.: Condens. Matter* **15** L749–54
[2] Cao Q P, Zhou Y H, Horsewell A and Jiang J Z 2003 *J. Phys.: Condens. Matter* **15** 8703–12
[3] Sikka S K 2004 *J. Phys.: Condens. Matter* **16** S1033–9
[4] Gioti M, Logothetidis S and Charitidis C 1998 *Appl. Phys. Lett.* **73** 184–6
[5] Logothetidis S, Gioti M and Kelires P C 1998 *J. Non-Cryst. Solids* **227–230** 1113–7
[6] Zeng H, Qui J, Jiang X, Zhu C and Gan F 2004 *J. Phys.: Condens. Matter* **16** 2901–6
[7] Inoue A 2000 *Acta Mater.* **48** 279–306
[8] Fan C, Li C and Inoue A 2000 *Phys. Rev.* B **61** R3761–3
[9] Jiang J Z, Roseker W, Jacobsen C S and Goya G F 2003 *J. Phys.: Condens. Matter* **15** 8713–8
[10] Duscher G, Mullejans H, Werner J and Ruhle M 1996 *Mater. Sci. Forum* **207–209** 713–6
[11] Mallamaci M P and Carter C B 1998 *Acta Mater.* **46** 2895–900
[12] Lee T-S, Gu G L and Tseng B-H 1996 Polycrystalline thin films: structure, texture, properties and applications II *MRS Symp. Proc.* vol 403, ed H J Frost, M A Parker, C A Ross and E A Holm (Pittsburg, PA: Materials Research Society) pp 119–24
[13] Park S, Chung Y, Qin W, Cho H, Cho E, Jang K, Kim S, Lee Y-I and Kim C 2004 *J. Phys.: Condens. Matter* **16** 2543–9
[14] Chen Y G and Liu B X 1997 *J. Phys. D: Appl. Phys.* **30** 510–6
[15] Verpek S and Argon A S 2002 *J. Vac. Sci. Technol.* B **20** 650–64
[16] Verpek S 2003 *Rev. Adv. Mater. Sci.* **5** 6–16
[17] Ovid'ko I A 1994 *J. Phys. D: Appl. Phys.* **27** 999–1007
[18] Gutkin M Yu and Ovid'ko I A 1999 *J. Phys.: Condens. Matter* **11** 8607–16
Gutkin M Yu and Ovid'ko I A 2001 *Phys. Rev.* B **61** 064515–23
[19] Herbert R J and Perepezko J H 2003 Nanomaterials for strucutral applications *MRS Symp. Proc.* vol 740, ed C C Berndt, T Fischer, I A Ovid'ko, T Tsakalakos and G Skandan (Pittsburg, PA: Materials Research Society) pp 267–72
[20] Benedictus R, Bottger A and Mittenmejer E J 1996 *Phys. Rev.* B **54** 9109–19
[21] Fitzgerald E A 1991 *Mater. Sci. Rep.* **7** 87–142
[22] Van der Merve J H 1991 *Crit. Rev. Solid State Mater. Sci.* **17** 187–209
[23] Jain S C, Harker A H and Cowley R A 1997 *Phil. Mag.* A **75** 1461–515
[24] Ovid'ko I A 1999 *J. Phys.: Condens. Matter* **11** 6521–7
Ovid'ko I A 2001 *J. Phys.: Condens. Matter* **13** L97–103
[25] Ovid'ko I A and Sheinerman A G 2002 *Phys. Rev.* B **66** 245309
Ovid'ko I A and Sheinerman A G 2003 *J. Phys.: Condens. Matter* **15** 2127–35
[26] Gutkin M Yu, Ovid'ko I A and Sheinerman A G 2000 *J. Phys.: Condens. Matter* **12** 5391–401
Gutkin M Yu, Ovid'ko I A and Sheinerman A G 2003 *J. Phys.: Condens. Matter* **15** 1173–81
[27] Ovid'ko I A 1999 *Phil. Mag. Lett.* **79** 709–13
[28] Ninomiya T 1983 *Topological Disorder in Condensed Matter* ed G Toulouse (Berlin: Springer) pp 40–50
[29] Nelson D R 1983 *Phys. Rev. Lett.* **50** 982–5
Nelson D R 1983 *Phys. Rev.* B **28** 5515–35
[30] Rivier N 1987 *Adv. Phys.* **36** 95–134
[31] Romanov A E and Vladimirov V I 1992 *Dislocations in Solids* vol 9, ed F R N Nabarro (Amsterdam: North-Holland) pp 191–402
[32] Gutkin M Yu, Ovid'ko I A and Romanov A E 1994 *Radiat. Eff. Defects Solids* **129** 239–55
[33] LeGoues F K, Copel M and Tromp R 1989 *Phys. Rev. Lett.* **63** 1826–9
LeGoues F K, Copel M and Tromp R 1990 *Phys. Rev.* B **42** 11690–700
[34] Ozkan C S and Nix W D 1997 *Appl. Phys. Lett.* **70** 2247–9
[35] Ovid'ko I A, Sheinerman A G and Skiba N V 2003 *J. Phys.: Condens. Matter* **15** 1173–81
[36] Sutton A P and Balluffi R W 1995 *Interfaces in Crystalline Materials* (Oxford: Clarendon)
[37] Shenderova O A, Brenner D W, Nazarov A A, Romanov A E and Yang L H 1998 *Phys. Rev.* B **57** R3181–4
[38] Bobylev S V, Ovid'ko I A and Sheinerman A G 2001 *Phys. Rev.* B **64** 224507
[39] Kleman M and Friedel J 1969 *J. Physique Coll.* IV **4** 43–53
[40] Mura T 1987 *Micromechanics of Defects in Solids* (Dordrecht: Martinus Nijhoff)
[41] Nold E, Steeb S and Lamparter P 1980 *Z. Naturf.* A **35** 610–2
[42] Smithells C J and Brands E A 1976 *Metals Reference Book* (London: Butterworth)
[43] Udler D and Seidman D N 1996 *Phys. Rev.* B **54** R11133–6
[44] Kröner E 1958 *Kontinuumstheorie der Versetzungen und Einenspannungen* (Berlin: Springer)
[45] Ditkin V A and Prudnikov A P 1974 *Integral Transforms and Operational Calculus* (Moscow: Nauka) (in Russian)